Efficient Solvation Free Energy Calculations of Amino Acid Analogs by Expanded Ensemble Molecular Simulation

Andrew S. Paluch,[†] Jindal K. Shah,[†,‡] and Edward J. Maginn*,[†]

[†]Department of Chemical and Biomolecular Engineering and [‡]Center for Research Computing, University of Notre Dame, Notre Dame, Indiana 46556, United States

S *Supporting Information*

ABSTRACT: We present an efficient, automated expanded ensemble method to calculate the residual chemical potential or solvation free energy by molecular dynamics simulation. The methodology is validated by computing the residual chemical potential of 13 amino acid analogs in water at 300 K and 1 bar and comparing to reference simulation data. Overall agreement is good, with the methodology of the present study reaching limiting precisions of less than 0.1 k_BT in half of the total simulation time of the reference simulation study which utilized Bennett's acceptance ratio method. The apparent difference in the efficiencies is a result of the inherent advantages of the expanded ensemble method, which creates an improved decorrelation of simulation data and improves the sampling of the important regions of the configurational phase space of each subensemble. The present adaptation utilizes histograms of proposed transition energies collected throughout the entire simulation, to make extremely precise calculations of the relative free energy between neighboring subensembles.

1. INTRODUCTION AND MOTIVATION

The thermodynamic behavior of all chemical and biological systems at equilibrium may be fundamentally understood in terms of the underlying free energy or chemical potential. Knowledge of the free energy is crucial to understanding the phase equilibria between solids, liquids, and gases, which in turn is key for the design of separation processes and the selection of solvents for synthesis reactions. Likewise, the transport of drug molecules between cell membranes and partitioning between multiple environments may be explained in terms of the relative chemical potentials, whose knowledge is crucial for drug design.[1] The importance of such information in drug design is emphasized by the fact that entire monographs have been devoted to the topic.[2,3]

Proteins are required by the body for the growth, repair, and maintenance of cells. They are vital for virtually every process within the human body, such as metabolism and digestion, and are necessary for the production of antibodies to fight off infections and diseases. Proteins may be regarded as large biopolymers of amino acids, creating an expansive range of possible chemical compositions.[4] Insight into the native structure and the folding mechanism of proteins in solution may be obtained by examining the solvation free energy of individual constituent amino acid analogs.[5,6]

To make the link between the solvation free energy of a given amino acid analog and a particular solvent, one must account for the molecular-level details that occur during solvation. One way to do this is via molecular simulation. Recently, several studies have looked at the ability of molecular simulation to predict hydration free energies of amino acid analogs.[7–11] All of the studies employed either thermodynamic integration (TI)[12] or Bennett's acceptance ratio (BAR) method,[13] and results were presented with an unprecedented level of precision.[7] Despite the success of the studies, all of the employed methods were computationally intensive. To facilitate the calculations, a stratification or staging strategy was used in which intermediate states were constructed in between the target and the reference state, so as to increase the phase space overlap between neighboring states.[14,15] That is, many simulations at varying coupling strengths of the amino acid analogs were conducted, followed by postsimulation data analysis.

An additional method that may help facilitate the exploration of phase space for computing solvation free energies is the expanded ensemble (EE) method originally developed by Lyubartsev and co-workers.[16–19] While the free energy between states is calculated with an appropriate technique, a single simulation is performed in which a random walk is constructed over the reference, intermediate, and target states. The phase space of each state is sampled according to a unique Hamiltonian, and the propagation of configurations between neighboring states helps prevent quasi-nonergodicity, improving the rate of exploration of phase space. The EE method has been combined previously with various techniques to compute free energy changes in an efficient, automated fashion[20–23] with a high level of precision.[24,25] In addition, the EE method has been applied to study the solvation free energies of drug molecules.[26] Together, these previous studies suggest that automated EE calculations may be applied to obtain precise solvation free energies of biological systems in an extremely efficient manner.

In the present study, we evaluate the use of EE to calculate the solvation free energy of amino acid analogs in an efficient, automated fashion, reaching levels of precision comparable to previous studies.[7,27] We have accomplished this by combining the strengths of the flat histogram method of Wang and Landau

(WL)[28−30] with the BAR technique. The approach extends our previous work[25] in two ways: First, the current implementation of EE is in a molecular dynamics (MD) framework rather than a Monte Carlo (MC) framework.[17] The choice of sampling configurational phase space with MD resulted from the overwhelming preference of the biological modeling community for MD versus MC as a means of generating configurations. Furthermore, the numerous, highly efficient, freely available MD codes reinforced this motive. Second, the current study employs BAR rather than transition-matrix Monte Carlo (TMMC).[31−35] This was done because BAR is straightforward to implement within MD. By using BAR, the method may be employed using either MC or MD. We note that TMMC and BAR have been shown to be intimately related,[36,37] and the MD implementation of EE[17] has similarities with the independently formulated λ-dynamics method.[38] In Section 2 of the paper we will present an overview of the employed methodology, followed by the relevant computational details in Section 3. Results and discussion are given in Section 4, followed by a summary of our findings in Section 5.

2. METHODS

EE. The main idea behind the EE method is to construct an augmented ensemble as a sum of subensembles.[16−19] This series of subensembles connects two systems of interest by gradually performing transitions between the two systems. In the current study, the systems of interest are pure solvent (water) and solvent with the addition of a single solute (amino acid analog) molecule at the same temperature and pressure. These systems are connected through a series of subensembles that begin with a noninteracting solute molecule in a pure solvent (i.e., an ideal gas reference state at the same density of the pure solvent) and end with a fully interacting solute molecule in solution. The intermediate subensembles serve to scale the intermolecular interaction potential of the solute. A specific subensemble is designated by index m. Intermolecular Lennard-Jones (LJ) and electrostatic (elec) interactions are regulated by the subensemble dependent coupling parameters λ_m^{LJ} and λ_m^{elec}, respectively, which vary from $0 \leq \lambda_m^{LJ} \leq 1$ and $0 \leq \lambda_m^{elec} \leq 1$.

While within a given subensemble, configurational phase space is sampled by MD. Periodically, a MC random walk is performed in which moves consist of transitions to neighboring subensembles. In this way, a probability distribution over subensembles is generated. In the isothermal−isobaric expanded ensemble (EE-NpT), a specific microstate (or configuration within a subensemble m) is observed with probability:

$$\pi_m(\mathbf{r}) = \frac{1}{Z_{NpT}} \exp\{-\beta[U_m(\mathbf{r}) + pV(\mathbf{r})]\} \quad (1)$$

where Z_{NpT} is the EE-NpT configurational partition function (or configurational integral), U_m is the subensemble dependent potential energy, p and V are the pressure and the volume, respectively, $\beta = 1/k_BT$, where k_B is Boltzmann's constant and T is the temperature, and $\mathbf{r}$ is a $3(N_{solv} + N_{solute})$ dimensional vector representing the positions of the solvent and solute molecules, where N_{solv} and N_{solute} are the number of solvent and solute molecules, respectively. Note that for all of the cases examined here $N_{solute} = 1$. A transition from subensemble m to

subensemble n is accepted with probability:[39]

$$a_{m \to n} = \min\left\{1, \frac{\pi_n(\mathbf{r})}{\pi_m(\mathbf{r})}\right\} \quad (2)$$

Transitions attempting to take the system outside the range of subensembles are rejected. Further, the probability Π_m of finding the system in a given macrostate (or subensemble m) is the sum over all microstates in the subensemble:

$$\Pi_m = \sum_{\mathbf{r}} \pi_m(\mathbf{r}) \quad (3)$$

The probability of visiting a macrostate is characterized by the configuration of the system and the subensemble. Thus, each microstate maps to a single macrostate. The relative Gibbs free energy between any two subensembles m and n is related to the relative macrostate probabilities as:[16−18]

$$\beta G_n(N_{solv}, N_{solute}, T, p) - \beta G_m(N_{solv}, N_{solute}, T, p)$$
$$= -\ln\left(\frac{\Pi_n}{\Pi_m}\right) \quad (4)$$

It follows from the definition of the chemical potential and finite difference arguments that[18]

$$\mu_{solute}^{res}(N_{solv}, N_{solute}, T, p) = -\ln\left(\frac{\Pi_{M_{Total}}}{\Pi_0}\right) \quad (5)$$

where μ_{solute}^{res} is the residual chemical potential of the solute (i.e., chemical potential of the solute relative to an ideal gas reference state), and the subscripts M_{Total} and 0 are the subensemble indices corresponding to the fully interacting solute in solution and the noninteracting solute in solution, respectively. The residual chemical potential is equivalent to the Gibbs free energy of transfer reported in many studies of biological systems.[7−9,11]

As a result of eq 4, we find that as the free energy difference between subensembles increases, the frequency of transitions between subensembles decreases exponentially. To ensure that the system sufficiently samples the entire range of subensembles, a subensemble dependent weighting function η_m is employed to bias the acceptance probability.[40] Trial moves between subensembles are accepted according to a biased acceptance probability:

$$a_{\eta, m \to n} = \min\left\{1, \frac{\pi_n(\mathbf{r})}{\pi_m(\mathbf{r})} \exp(\eta_n - \eta_m)\right\} \quad (6)$$

A uniform sampling of subensembles is obtained if the weighting functions are set according to

$$\eta_n - \eta_m = -\ln\left(\frac{\Pi_n}{\Pi_m}\right) \quad (7)$$

Unfortunately, Π_n and Π_m are the unknown macrostate probabilities that one seeks to calculate and, in general, are not known a priori. In the original implementation of the EE method,[16−19] a multicanonical algorithm[41] was adopted to estimate the weighting functions in an iterative manner through a series of short simulations until a relatively flat visited states histogram was achieved. Advances have been made with the use of histogram based methods that aim to calculate directly the macrostate probabilities with a high level of precision and obtain the relevant

1395

dx.doi.org/10.1021/ct1006746 |J. Chem. Theory Comput. 2011, 7, 1394–1403

weights by use of eq 7. These histogram methods include WL and TMMC and the intimately related BAR.[36,37,42] Recent studies have also successfully combined multiple methods, namely WL and TMMC.[25,43] In the present study, we will employ a combined WL-BAR approach, as described in the next subsection.

WL-BAR Scheme. To obtain an initial estimate of the weighting functions in eq 6, WL is used to estimate the macrostate probability and hence the weighting functions via eq 7. The EE-NpT simulation is started with the phase space of each subensemble being sampled by MD, and periodic attempts are made to transition between subensembles. After each attempted transition, the current estimate of the macrostate probability is updated as

$$\ln \Pi_m^{\text{new}} = \ln \Pi_m^{\text{old}} + v_{\text{WL}} \qquad (8)$$

where v_{WL} is a convergence factor greater than 0. After a specified period of time, the convergence factor is reduced according to the following expression:

$$v_{\text{WL}}^{\text{new}} = \kappa \cdot v_{\text{WL}}^{\text{old}} \qquad (9)$$

where κ is an update factor less than 1. The entire process is then repeated. The implementation of WL has been studied extensively in the past,[28−30,44,45] including a detailed discussion with regards to combining WL with TMMC.[43] Given the close resemblance of TMMC and BAR,[36,37,42] we have followed the recommendations of Shell et al.[43] Namely, the convergence factor should initially be large enough to sample a broad range of subensembles, allowing for the collection of an expansive amount of transition energies. However, the convergence factor should not be excessively large and should then be quickly reduced, minimizing the time and the extent at which our random walk violates detailed balance. The heuristics of this update scheme are provided in the next section.

The WL procedure quickly samples a broad range of subensembles but converges to a limiting, nonprecise estimate of the macrostate probabilities that are not improved with additional steps.[29] On the other hand, TMMC and BAR methods may be slower to sample a broad range of subensembles[35] but converge upon an extremely precise estimate of the macrostate probabilities.[34,36] Therefore, in an effort to utilize the strengths of both WL and BAR, after sufficient sampling has been achieved with WL, the WL calculated weights are refreshed with weights calculated with BAR. It is important to emphasize that the role of WL is only to quickly sample a broad range of macrostates; the free energy is ultimately calculated using BAR.

BAR is an optimal method to calculate free energy differences between neighboring states and has been derived previously using several different criteria: by minimizing the variance of the acceptance ratio between neighboring states,[13,46] as an optimal overlap-sampling method,[47] and by using maximum likelihood arguments.[48] In addition, Ferrenburg and Swendsen[49] showed that the optimal combination of histogram data reduces to BAR in the limit that only two states are sampled. Also, Escobedo and co-workers[36,37] have shown that TMMC is a limiting case of BAR. As a result of the many derivations in previous studies, only the relevant working equations will be presented here. To calculate the free energy difference between subensembles n and m, BAR considers perturbations from both m to n and n to m.

The difference in free energy is then calculated as

$$\beta G_n(N_{\text{solv}}, N_{\text{solute}}, T, p) - \beta G_m(N_{\text{solv}}, N_{\text{solute}}, T, p)$$

$$= -\ln \left[\frac{\langle f(U_n - U_m - C)\rangle_m}{\langle f(U_m - U_n + C)\rangle_n} \right] + \beta C \qquad (10)$$

where $f(x)$ is the Fermi−Dirac function $[1 + \exp(\beta x)]^{-1}$, C is an adjustable parameter, and the brackets correspond to an ensemble average taken with respect to the probability distribution of subsemble n or m, as indicated by the subscript. While in principle any value of C may be used,[13] the optimal value is found by the following relationship:

$$\sum_{N_{n \to m}} f(U_m - U_n + C) = \sum_{N_{m \to n}} f(U_n - U_m - C) \qquad (11)$$

where $N_{n \to m}$ and $N_{m \to n}$ are the number of perturbations from n to m and m to n, respectively. During the course of the simulation, histograms are collected to track the transition energies (i.e., $U_n - U_m$) between each subensemble. While configurations (and hence energies) are correlated for a finite time, when a transition is accepted, the system begins sampling from a different Hamiltonian. This transitioning reduces the configurational correlation time of the system relative to a simulation in a fixed ensemble.

Periodically, an estimate of the free energy difference between neighboring subensembles is calculated by self-consistently solving eq 11 and then using eq 10 to obtain the free energy difference. From eqs 4 and 7, the free energy difference may be used as a new estimate of the weighting functions. While the weighting functions are continuously changing, the transition energies required for BAR are continuously collected from the unbiased target and reference subensembles. In this way, the transition energy histograms do not need to be rezeroed.[31,33,36] Physical insight into the success of BAR is presented nicely in the work of Kofke and co-workers,[47,50,51] who present BAR as an optimized overlap sampling method. Rather than viewing BAR in the context of a perturbation from both m to n and n to m, it is better viewed as a two stage perturbation in which perturbations in each direction are performed to a mutual intermediate state. The optimized BAR will select an intermediate state between the two neighboring states that is inside the overlapping region of their respective phase spaces; the free energy prediction from BAR is then the sum of the free energy difference between each neighbor and the intermediate state.[47,50,51] Therefore, so long as there exists a phase space overlap, with sufficient sampling, BAR will be successful.

3. COMPUTATIONAL DETAILS

Molecular Models. To model the intermolecular and intramolecular interactions of the systems, a proper force field is required. While many models exist, it was not the objective of the present work to evaluate which models reproduce experimental data the best. Rather, the objective was to test the simulation method itself, and therefore models were selected to allow for comparison with previous work of Dill and co-workers.[27] Consistent with that work, water was modeled with the rigid three-point transferable intermolecular potential function (TIP3P) of Jorgensen and co-workers.[52] Parameters for the amino acid analogs were taken from the general AMBER force field (GAFF)[53,54] with AM1-BCC partial charges.[55] A complete listing of parameters may be found in the Supporting Information of the paper

1396

dx.doi.org/10.1021/ct1006746 |*J. Chem. Theory Comput.* 2011, 7, 1394–1403

Table 1. Studied Amino Acid Analogs and the Corresponding Amino Acid

amino acid	analog
NH$_2$(R)CHCOOH	RH
Ala	methane
Val	propane
Ile	n-butane
Leu	isobutane
Ser	methanol
Thr	ethanol
Phe	toluene
Tyr	p-cresol
Cys	methanethiol
Met	methylethylsulfide
Asn	acetamide
Trp	3-methylindole
His	4-methylimidazole

by Dill and co-workers.[27] The studied amino acid analogs and the corresponding amino acids are summarized in Table 1. In all of these cases, nonbonded intermolecular interactions were treated using a combined LJ and fixed point charge model of the form:

$$U_{nb}(r_{ij}) = 4\varepsilon_{ij}\left[\left(\frac{\sigma_{ij}}{r_{ij}}\right)^{12} - \left(\frac{\sigma_{ij}}{r_{ij}}\right)^{6}\right] + \frac{1}{4\pi\varepsilon_0}\frac{q_i q_j}{r_{ij}} \quad (12)$$

where r_{ij}, ε_{ij}, σ_{ij}, q_i, and q_j are the site separation distance between atoms i and j, well-depth of the LJ interaction, distance at which the LJ interaction is zero, and partial charge values, respectively. For interactions between unlike LJ sites, Lorentz−Berthelot combining rules[39] were employed. To prevent instabilities in the trajectory when the solute is nearly decoupled from the system (i.e., when $\lambda_m^{LJ} \approx 0$), solute−solvent intermolecular nonbonded LJ interactions were modeled with a modified, "soft-core" potential of the form:[8,56,57]

$$U_{LJ}^{sc}(r_{ij}; m)$$

$$= 4\lambda_m^{LJ}\varepsilon_{ij}\left\{\frac{\sigma_{ij}^{12}}{[(1-\lambda_m^{LJ})\alpha_{LJ}\sigma_{ij}^6 + r_{ij}^6]^2} - \frac{\sigma_{ij}^6}{[(1-\lambda_m^{LJ})\alpha_{LJ}\sigma_{ij}^6 + r_{ij}^6]}\right\} \quad (13)$$

where r_{ij}, ε_{ij}, and σ_{ij} are the same LJ parameters as in eq 12, λ_m^{LJ} is the subensemble dependent coupling strength of the LJ potential, and α_{LJ} is a constant, taken in this study to be 1/2. Note that when the solute molecule is fully coupled to the system, $\lambda_m^{LJ} = 1$, and eq 13 reduces to the normal LJ potential given by eq 12. When the solute is nearly decoupled, λ_m^{LJ} approaches 0, and eq 13 represents a smooth interaction function that allows solvent molecules to overlap the solute with finite energy. When the solute is decoupled from the system, $\lambda_m^{LJ} = 0$, and the potential is 0. Thus, the potential form in eq 13 correctly represents the limiting behavior of the solute−solvent interactions, while eliminating instabilities when λ_m^{LJ} approaches 0. Solute−solvent intermolecular electrostatic interactions are decoupled linearly as

$$U_{elect}(r_{ij}; m) = \lambda_m^{elect}\frac{1}{4\pi\varepsilon_0}\frac{q_i q_j}{r_{ij}} \quad (14)$$

where r_{ij}, q_i, and q_j are the same as in eq 12, and λ_m^{elec} is the subensemble dependent coupling strength of the electrostatic interactions.

The same standard LJ and electrostatic interaction potentials (eq 12) and combining rules are used for all intramolecular nonbonded interactions by all pairs of atoms separated by three or more bonds. For the case in which the intramolecular sites are separated by exactly three bonds, the LJ and electrostatic interactions are scaled by a factor of 1/2 and 5/6, respectively.

While the TIP3P water model is completely rigid, the amino acid analogs were modeled with fixed bond lengths but flexible bond and dihedral angles. The bond angle bending intramolecular interaction between sites separated by two bonds was modeled by a simple harmonic potential of the form:

$$U_{angle}(\theta_{ijk}) = k_{ijk}(\theta_{ijk} - \theta_{ijk}^0)^2 \quad (15)$$

where k_{ijk}, θ_{ijk}, and θ_{ijk}^0 are the force constant, angle between sites i, j, and k, and corresponding nominal bond angle, respectively. The torsional potential describing the intramolecular interaction between sites separated by three bonds was modeled by a potential of the form:

$$U_{tors}(\varphi_{ijkl}) = \sum_{n=0}^{5} K_n \cos^n(\varphi_{ijkl} - 180^o) \quad (16)$$

where ϕ_{ijkl} is the dihedral angle between sites i, j, k, and l, and the K_n coefficients are constants. The same torsional potential form was used to describe improper dihedral angles, meant to keep planar groups planar. All of the amino acid analog force field files used in the present study are provided in the Supporting Information.

Simulation Details. All simulations were performed with a modified version of the MD simulation package M.DynaMix 5.2.[58,59] For all systems studied in this work, LJ interactions were truncated at a distance of $r_{cut} = 12$ Å, and standard uniform fluid tail corrections were applied to both the energy and the pressure, assuming $g(r) = 1$ beyond the cutoff.[39,46] Electrostatic interactions were evaluated with an Ewald summation with tin foil boundary conditions,[39,46] with real space interactions truncated at r_{cut}. A damping parameter of $\alpha r_{cut} = 3.72$ was used, and the maximum number of reciprocal space lattice vectors was set by $K_{max} = 11.0$. Integration of the equations of motion was performed with the Verlet leap-frog algorithm in Cartesian coordinates[39,46] with a time step of 2 fs. All bond lengths and the H−O−H angle of water were constrained with the SHAKE algorithm[60] with a tolerance of 10^{-6}. An Andersen thermostat,[61] as implemented by Andrea et al.,[62] and Andersen−Hoover barostat[61,63] were used to sample the phase space of an isothermal−isobaric (NpT) ensemble at 300 K and 1 bar. The collision time for the thermostat was set at 0.4 ps, and the time constant for the barostat was 1.5 ps. Modifications to M. DynaMix include implementation of the Andersen thermostat, the "soft-core" potential (eq 13), separate decoupling of LJ and electrostatic interactions for EE calculations, WL-BAR, modification of the Ewald summation with EE solute molecules as described in the Appendix, and other minor additions.

The systems were set up by randomly placing a single gas phase minimized solute molecule in each of the five independently equilibrated cubic boxes of 900 TIP3P water molecules. Production runs were carried out in an EE-NpT ensemble at 300 K and 1 bar for a total of 10 ns. Each of the five independent systems were initialized with a unique random number seed for the thermostat and for the MC random walk, with all velocities
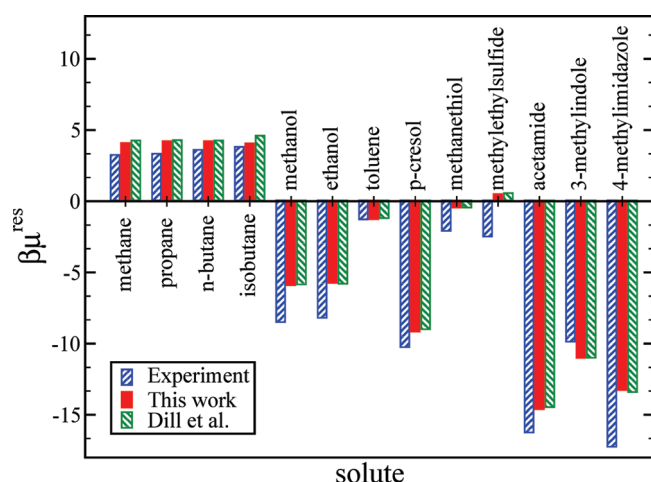
Figure 1. Comparison of the residual chemical potential ($\beta\mu^{\text{res}}$) of the 13 studied amino acid analogs (solutes) from experiment,[67] computed in this study and reference simulation results of Dill and co-workers.[27]

initialized from a Maxwell−Boltzmann distribution at 300 K. The system began in the subensemble with a noninteracting solute molecule and attempts to change subensembles were made every 10 fs. Over the first 0.5 ns, the random walk was carried out with WL biasing, in which the WL weight factor was initially taken to be $v_{\text{WL}} = 0.25$ and reduced as $v_{\text{WL}}^{\text{new}} = 0.25 v_{\text{WL}}^{\text{old}}$ every 0.1 ns. The initial WL weight factor was chosen to be an order of magnitude smaller than $\mathscr{O}\,(1)$ values typically used,[28−30,44,45] yet large enough to sample a broad range of subensembles. The update scheme quickly reduced the weight factor to a value of 0.004 after 0.4 ns for the last WL biasing cycle. During the entire course of the simulation, transition energies (in both directions) were computed each time a transition between subensembles was attempted/ proposed, and new subensemble weights were computed from BAR every 0.5 ns. The solute was taken from noninteracting ($m = 0$) to fully interacting ($m = 20$) by first bringing the intermolecular LJ interaction to full strength over 15 subensembles ($1 \leq m \leq 15$) and then adding in intermolecular electrostatic interactions in the final five subensembles ($16 \leq m \leq 20$), for a total of 20 subensembles. For the first 15 subensembles, the intermolecular electrostatic interactions were turned off, and the intermolecular LJ interactions were strengthened as $\lambda_m^{\text{LJ}} = \{0.05, 0.10, 0.20, 0.30, 0.40, 0.50, 0.60, 0.65, 0.70, 0.75, 0.80, 0.85, 0.90, 0.95, 1.0\}$. Next, while the LJ intermolecular interactions were fully restored, the intermolecular electrostatic interactions were strengthened as $\lambda_m^{\text{elec}} = \{0.2, 0.4, 0.6, 0.8, 1.0\}$. Care must be taken to properly decouple the solute−solvent intermolecular interactions with Ewald summation; a detailed description of how this was done is given in the Appendix.

The reported residual chemical potentials of the present work are the mean value of the five independent productions runs for each solute, and the uncertainty is taken as the bootstrap standard error.[64−66] To compute the bootstrap standard error for each solute−solvent combination, the estimate of the chemical potential from each of the five production runs was taken to be an independent data point. Next, 1000 sets containing 5 data points each were created by randomly selecting 5 of our independent data points, with replacement. The mean of each set was computed, creating a bootstrap sample of 1000 estimates of the residual chemical potential. The bootstrap standard error

was then found as the standard error of the bootstrap sample relative to the mean of the five independent production runs for each solute−solvent combination.

4. RESULTS AND DISCUSSION

A summary of the computed residual chemical potentials and a comparison to experiment[67] and the simulation work of Dill and co-workers[27] are provided in Figure 1 and in Table 2. The results of the present study are in good overall agreement with the previous simulation results, with an average absolute difference between the computed residual chemical potentials of the present study and Dill and co-workers[27] of 0.13 $k_{\text{B}}T$. If we exclude isobutane from this calculation, which will be discussed in further detail, the average difference decreases to 0.09 $k_{\text{B}}T$, which is the same order of magnitude of the reported uncertainties. The excellent agreement of the results suggests that the proposed method yields correct residual chemical potentials. In all cases, an estimate of the residual chemical potential may be obtained within a few ns of simulation time. Further time beyond this serves only to decrease the uncertainty of the calculation.

The largest discrepancy between the present study and that of Dill and co-workers[27] is found for isobutane, corresponding to a discrepancy of 0.53 $k_{\text{B}}T$, which warrants further investigation. While results of EE calculations are not known to be biased, a potential source of error in the calculations may result from a lack of configurational phase space overlap between neighboring states;[50,51,68,69] the degree of phase space overlap between neighboring states is related to the relative entropy and the energy histograms between neighboring states,[50,51] and for the case of EE, it is related to the observed visited states[16,17] and transition[20] probabilities. As mentioned previously, BAR is limited to applications in which neighboring states have at least some phase space overlap. So long as the states have some phase space overlap, with sufficient sampling, BAR will select an intermediate state between the two neighboring states that is inside the overlapping region of their respective phase spaces; the free energy prediction from BAR is then the sum of the free energy difference between each neighbor and the intermediate state.[47,50,51] Therefore, if there is little or no phase space overlap, BAR will be unsuccessful, and we would expect there to be little or no transitions between neighboring subensembles. The result would be a relatively large uncertainty in the predicted residual chemical potential between independent simulations stemming from inadequate sampling.

To this end, Figure 2 shows the observed visited state and transition probabilities for our EE simulation of isobutane. In the bottom pane it is observed that in all cases, the forward transition probability from subensemble m to subensemble $m + 1$ is nearly indistinguishable from the reverse transition probability to subensemble m from subensemble $m + 1$. Therefore, as a result of MC detailed balance,[39] there is nearly a uniform probability of visiting each subensemble, as shown in the top panel. In addition, the observed transition probabilities are fairly high, between 20 and 50%, ensuring an adequate sampling of each subensemble. As shown in Table 2 and Figure 3, the predicted free energy for isobutane converges to a limiting value with a precision of 0.09 $k_{\text{B}}T$, dismissing concerns with regards to phase space overlap.

Furthermore, in Figure 4 we can compare to the results of Pande and co-workers[7] who employed the same TIP3P water model but used a previous version of the AMBER force field and a different treatment of long-range electrostatic interactions.

Table 2. Summary of the Residual Chemical Potential ($\beta\mu^{res}$) of the 13 Studied Amino Acid Analogs (Solutes) from Experiment,[67] Computed in This Study, and Reference Simulation Results of Dill and Co-Workers[27] [a]

solute	amino acid	$\beta\mu^{res}$			
		experiment[67]	this work	Dill et al.[27]	absolute difference
methane	Ala	3.25	4.09 ± 0.03	4.26 ± 0.02	0.17 ± 0.04
propane	Val	3.34	4.22 ± 0.05	4.29 ± 0.03	0.07 ± 0.06
n-butane	Ile	3.61	4.22 ± 0.08	4.26 ± 0.03	0.04 ± 0.08
isobutane	Leu	3.82	4.07 ± 0.09	4.60 ± 0.03	0.53 ± 0.09
methanol	Ser	−8.49	−5.89 ± 0.04	−5.84 ± 0.02	0.05 ± 0.04
ethanol	Thr	−8.19	−5.73 ± 0.04	−5.79 ± 0.05	0.06 ± 0.06
toluene	Phe	−1.27	−1.26 ± 0.05	−1.19 ± 0.03	0.07 ± 0.06
p-cresol	Tyr	−10.25	−9.16 ± 0.08	−8.99 ± 0.03	0.17 ± 0.08
methanethiol	Cys	−2.08	−0.33 ± 0.01	−0.44 ± 0.02	0.11 ± 0.02
methylethylsulfide	Met	−2.48	0.51 ± 0.04	0.57 ± 0.03	0.06 ± 0.05
acetamide	Asn	−16.24	−14.61 ± 0.05	−14.46 ± 0.05	0.15 ± 0.07
3-methylindole	Trp	−9.86	−11.01 ± 0.07	−10.99 ± 0.05	0.02 ± 0.09
4-methylimidazole	His	−17.24	−13.26 ± 0.04	−13.40 ± 0.05	0.14 ± 0.06

[a] The last column is the absolute difference of the present study relative to Dill and co-workers,[27] with the uncertainty computed from propagation of errors.
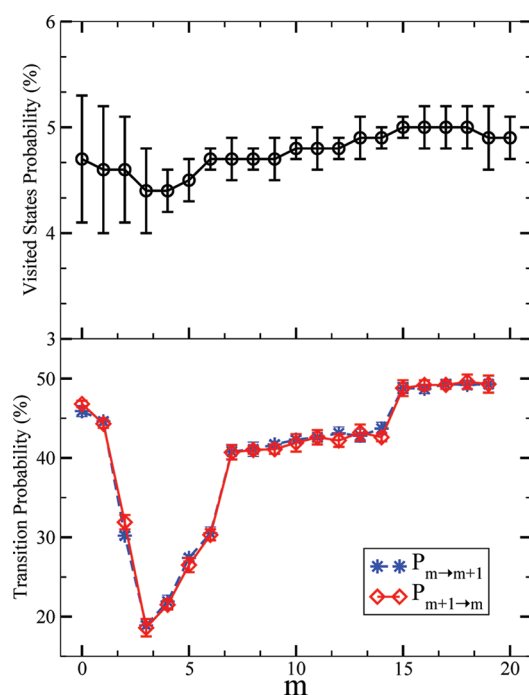

Figure 2. Summary of the observed visited states (top) and forward and reverse transition probabilities (bottom) for the EE simulations of isobutane as a function of subensemble m. For forward transition probabilities, the x-axis refers to the subensemble the transition is attempted from. For reverse transition probabilities, the x-axis refers to the subensemble the transition is attempted to. The error bars are the standard deviation of five independent simulations.

While we would not expect quantitative agreement, for alkanes in which the electrostatics interactions have a small contribution to the overall free energy, we would expect qualitative agreement. The observed trends for the alkanes in both the present study and that of Pande and co-workers[7] are consistent. Both studies observe that the solvation free energy of methane is less than
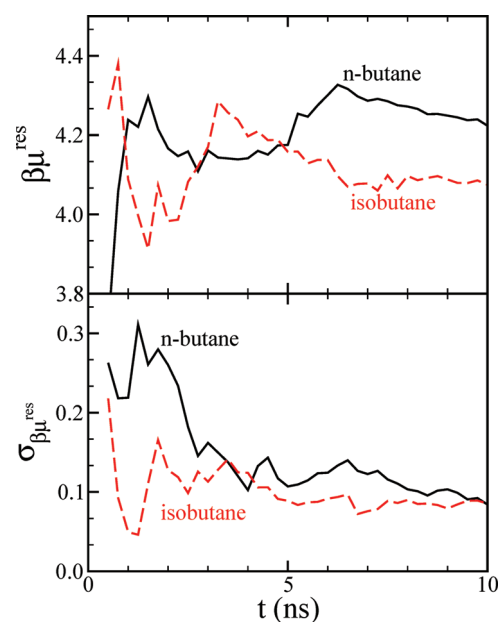

Figure 3. Performance of the EE method for predicting the residual chemical potential ($\beta\mu^{res}$) of n-butane and isobutane. The top panel is the estimate of the residual chemical potential as a function of simulation time, and the bottom pane is the boot strap standard error[64−66] of the five independent simulations as a function of simulation time.

propane and that of isobutane is less than n-butane. This observation is contrary to the results of Dill and co-workers.[27] This suggests that perhaps the uncertainty of the present results and for those of Dill and co-workers[27] may be larger than reported.

Overall, given the good agreement between the present study and that of Dill and co-workers,[27] we next draw our attention to evaluating the efficiency of the methodology employed in the current study. Figures 3 and 5−7 show the convergence of eight representative compounds from the current study. At the end of
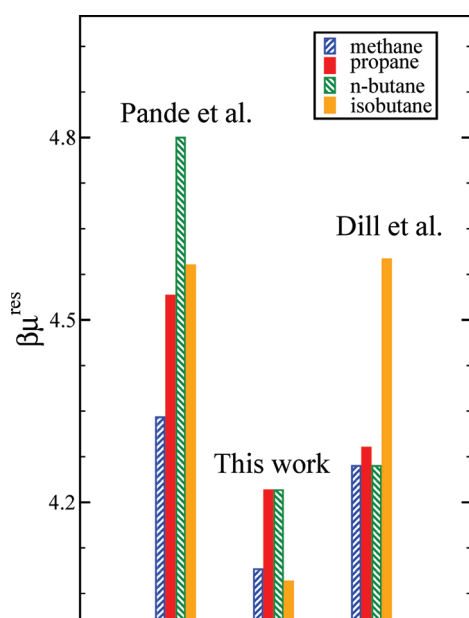
Figure 4. Comparison of the computed residual chemical potential ($\beta\mu^{res}$) of the four alkane molecules from Pande and co-workers,[7] this study, and Dill and co-workers.[27] Pande and co-workers[7] employed the same TIP3P water model but used a previous version of the AMBER force field and a different treatment of long-range electrostatic interactions.
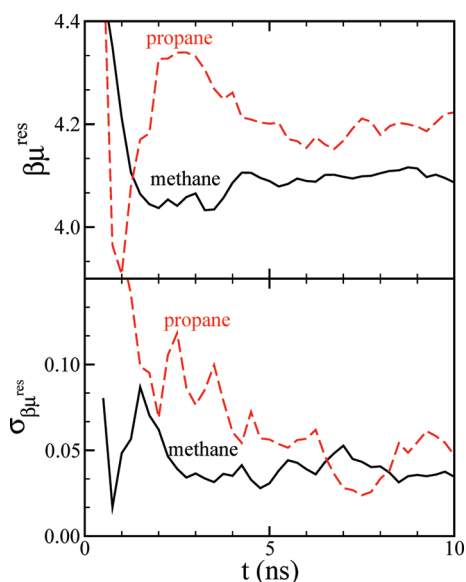

Figure 6. Performance of the EE method for predicting the residual chemical potential ($\beta\mu^{res}$) of methanethiol and methylethylsulfide. The top panel is the estimate of the residual chemical potential as a function of simulation time, and the bottom panel is the boot strap standard error[64−66] of the five independent simulations as a function of simulation time.

Figure 5. Performance of the EE method for predicting the residual chemical potential ($\beta\mu^{res}$) of methane and propane. The top panel is the estimate of the residual chemical potential as a function of simulation time, and the bottom panel is the boot strap standard error[64−66] of the five independent simulations as a function of simulation time.

Figure 7. Performance of the EE method for predicting the residual chemical potential ($\beta\mu^{res}$) of 4-methylimidazole and acetamide. The top panel is the estimate of the residual chemical potential as a function of simulation time, and the bottom panel is the boot strap standard error[64−66] of the five independent simulations as a function of simulation time.

the 10 ns simulation, all of the systems have converged to final residual chemical potentials (or hydration free energies) in agreement with Dill and co-workers[27] and with comparable precision. In the BAR study of Dill and co-workers,[27] independent simulations needed to be performed in each subensemble. Throughout the course of each simulation, transitions energies were periodically collected, and the free energy difference was
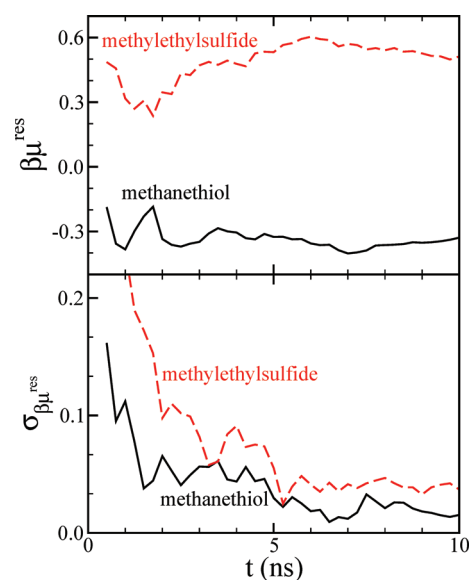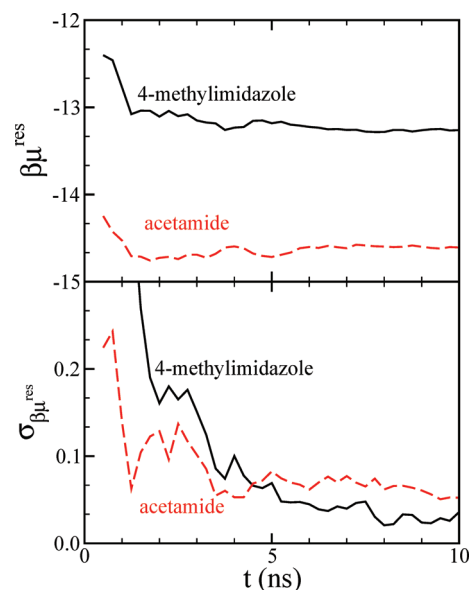
computed postsimulation using all of the collected data. While the present study utilized 5 independent, 10 ns simulations, the work of Dill and co-workers[27] required a 5 ns simulation at each of the 20 coupling strengths used. Therefore, the current study required half of the total simulation time, reducing the computational time by a factor of 2. Both studies used the same LJ scaling

1400

dx.doi.org/10.1021/ct1006746 |*J. Chem. Theory Comput.* 2011, 7, 1394–1403

and number of LJ subensembles, and both used the same linear, evenly spaced electrostatic scaling scheme, but the present study used an extra electrostatic subensemble. With the close agreement of the scaling and staging schemes, we will focus our attention on the employed methods themselves. Given the similarities of the two methods, namely both sampled configurational space with MD and employed similar BAR algorithms to calculate the free energy, a natural question arises: What is the source of the apparent difference in efficiencies of the two studies? The answer to this question gives insight into the clear advantages of employing EE in a MD framework.

First, equilibrium MD studies using BAR are limited by the configurational correlation time of the system. On the other hand, in the present study, subensemble transitions are periodically attempted. When a transition is accepted, the system begins sampling in a different subensemble. This transitioning reduces the configurational correlation time of the system and increases the rate of phase space sampling, akin to parallel tempering (or replica exchange) simulations.[70−72]

Second, in order for BAR to be successful, all of the important phase space of the target and reference subensemble need to be sampled.[15,47,50,51,68,69] In addition to stratification, the use of an importance weighted[14] MC sampling procedure[39] allows the system to bridge free energy barriers separating neighboring subensembles. This is accomplished by weighting the subensemble transition acceptance probabilities so as to artificially enhance the occurrence of important configurations of intrinsically low probability. Put differently, within a given subensemble, there are likely important regions of phase space of low probability of being observed or separated from other important regions by large energetic barriers. If we again draw analogy to parallel tempering (or replica exchange),[70−72] in subensembles in which we sample from a different Hamiltonian, these states may be sampled with a much greater probability. By importance weighting the transition acceptance probabilities, the likelihood of propagating these configurations is enhanced.

In addition to the theoretical advantages mentioned, although not utilized in the present study, the EE method with BAR is readily amenable to parallel processing. The present study utilized 5 independent 10 ns simulations for a total of 50 ns of simulation time. The MD BAR method of Dill and co-workers[27] required 20 independent 5 ns simulations or 100 ns of total simulation time. As all of the MD BAR simulations are independent from each other, with sufficient computational resources, they could be performed faster in real time using multiple processors. However, for the EE method the range of subensembles studied may be broken into various overlapping windows, in which an independent simulation may be conducted. Within each window the relevant free energy change may be calculated, and then all of the results may be stitched together by enforcing that the free energy be a continuous function of subensemble.[73,74] With an intelligent choice of windowing, the wall clock time necessary to calculate the residual chemical potential with EE may be readily decreased.[25]

Another advantage of the EE method is that it requires a single simulation whose convergence can be monitored during the simulation. Once the desired level of uncertainty is reached, the simulations may be terminated. For example, many of the simulations of the present study could have been stopped after 5 ns, and the precision would not have suffered (see Figures 3 and 5−7). The fact that no postprocessing is required to obtain a solvation free energy makes the method particularly easy to use.

5. CONCLUSION

Results have been presented for a refined expanded ensemble[16−19] algorithm that combines the flat histogram method of Wang and Landau[28−30] with the Bennett's acceptance ratio methodology[36,37,42] in a MD framework. The methodology was inspired by our previous success[25] with a combined transition-matrix Monte Carlo[31−35] and Wang−Landau approach. Use of the Bennett's acceptance ratio methodology is advantageous as a result of the ability to implement the methodology in either a MC or MD framework. The method was validated by computing the residual chemical potential of 13 amino acid analogs and by comparing to reference simulation data.[27] Overall agreement is good, with the methodology of the present study reaching a comparable precision in half of the total simulation time of the previous study.[27] The apparent difference in the efficiencies is a result of the inherent advantages of the expanded ensemble method. The proposed method creates an improved decorrelation of simulation data and enhances the sampling of the important regions of the configurational phase space of each subensembles. Furthermore, the present method enables the solvation free energy to be computed from a single simulation with no postprocessing. The encouraging results of the present study suggest consideration of the employed methodology in future studies requiring free energy calculations. Moreover, the proposed methodology is highly adaptable and may be used in any type of multicanonical framework.

■ APPENDIX

Ewald Summation with Expanded Ensemble. While the use of the Ewald sum for electrostatic interactions in molecular simulations has been described extensively in the literature,[39,46,75,76] we will briefly overview the necessary implementation when decoupling electrostatic interactions of a solute molecule using the EE method. With the EE method, modifications to the standard Ewald sum are necessary to ensure that electrostatic interactions are properly decoupled such that solute−solvent interactions are treated with scaled charges of the solute (corresponding to a given coupling strength), while intramolecular interactions are treated with unaltered charge interactions.

For charge neutral systems that are periodic in three dimensions, the electrostatic potential energy, U_{elect}, may be divided into four parts with the Ewald summation:

$$U_{elect} = \frac{1}{4\pi\varepsilon_0}[U_{real} + U_{recip} + U_{intra-self} + U_{point-self}] \quad (17)$$

where U_{real} and U_{recip} are the real- and reciprocal-space terms, respectively, and $U_{intra-self}$ and $U_{point-self}$ are the intramolecular- and point-self energies, respectively.

The real-space term is given by

$$U_{real} = \frac{1}{2}\sum_{i=1}^{N}\sum_{j=1}^{N\dagger} q_i q_j \frac{\text{erfc}(\sqrt{\alpha}r_{ij})}{r_{ij}} \quad (18)$$

where α is the damping parameter, and N is the total number of charge sites. The "dagger" ($\dagger$) summation indicates the exclusion of all pairs $i = j$, and intramolecular interactions separated by one, two, and three bonds. When evaluating the real-space term, all intramolecular electrostatic interactions separated by more than three bonds and all intermolecular electrostatic interactions involving only solvent molecules are treated with full charges,

and all intermolecular electrostatic interactions between the solute and solvent are treated with scaled charges.

The general form of the reciprocal-space term is given by

$$U_{\text{recip}}^{\text{general}} = \frac{2\pi}{V} \sum_{k \neq 0} \frac{1}{k^2} \exp\left(-\frac{k^2}{4\alpha}\right) \left[\left| \sum_{i=1}^{N} q_i \cos(\mathbf{k} \cdot \mathbf{r}_i) \right|^2 \right.$$
$$\left. + \left| \sum_{i=1}^{N} q_i \sin(\mathbf{k} \cdot \mathbf{r}_i) \right|^2 \right] \qquad (19)$$

where $\mathbf{r}_i$ is the position vector of site i, and $\mathbf{k}$ is the reciprocal lattice vector of the periodic cell images. Regardless if scaled or full charges are used for the solute molecule, eq 19 will be inconsistent with the real-space term in which different charges are used for intramolecular and intermolecular interactions. As a result, eq 19 is extended to involve three contributions:

$$U_{\text{recip}} = U_{\text{recip}}^{\text{scaled}} + U_{\text{recip}}^{\text{solute,full}} - U_{\text{recip}}^{\text{solute,scaled}} \qquad (20)$$

where the first term $U_{\text{recip}}^{\text{scaled}}$ is the evaluation of eq 19 using the actual intermolecular charges of the system. That is, the charges are full for the solvent and are scaled for the solute. To remain consistent with the formulation of the Ewald sum, the last two additional terms correct for different charges used for the intramolecular and intermolecular electrostatic interactions of the solute. $U_{\text{recip}}^{\text{solute,full}}$ is the evaluation of eq 19 but using full charges for the solute and performing the sine and cosine sum over all of the charge sites of the solute molecule (not the entire system). Similarly, $U_{\text{recip}}^{\text{solute,scaled}}$ is the evaluation of eq 19 but using scaled charges for the solute and performing the sine and cosine sum over all of the charge sites of the solute molecule. These additional two terms may be thought of as computing the reciprocal-space term for a system containing only the solute molecule at the same position, with both full and scaled charges. In the absence of interactions with the solvent, the difference of these two terms, $U_{\text{recip}}^{\text{solute,full}} - U_{\text{recip}}^{\text{solute,scaled}}$, gives the desired net effect of using different intermolecular and intramolecular charges. The necessary corrections to eq 19 may readily and efficiently be implemented into existing reciprocal-space Ewald subroutines with minor modifications. In addition, the extension to applications of particle-mesh Ewald[46] is straightforward.

The intramolecular-self energy is given by

$$U_{\text{intra-self}} = -\frac{1}{2} \sum_{j=1}^{M} \sum_{k=1}^{N_j} \sum_{l=1}^{N_j \dagger^{-1}} q_k q_l \frac{\text{erf}(\sqrt{\alpha} r_{kl})}{r_{kl}} \qquad (21)$$

where M is the total number of molecules in the system, and N_j is the number of charge sites on molecule j. The "inverse dagger" $(\dagger^{-1})$ summation indicates that the sum is only over intramolecular sites excluded in the real-space term of eq 18 (i.e. intramolecular interactions separated by one, two, and three bonds). While it is straightforward to exclude these terms in the real-space term in the central simulation cell, they are implicitly included in the reciprocal-space term. Equation 21 corrects the reciprocal-space term by removing these interactions.[76] Since all intramolecular interactions use full charges, full charges are used in eq 21.

Lastly, the point-self energy is given by

$$U_{\text{point-self}} = -\sqrt{\frac{\alpha}{\pi}} \sum_{i=1}^{N} q_i^2 \qquad (22)$$

Similar to the intramolecular self energy, the point self energy corrects the reciprocal space term for self interactions. That is, interactions of a charge site with itself are straightforward to exclude in the real-space term in the central simulation cell, but they are implicitly included in the reciprocal-space term. Therefore, eq 22 corrects the reciprocal-space term by removing these interactions.

For completeness, many force fields, including those used in the present study for the amino acid analogs, use scaled electrostatic interactions between intramolecular sites separated by exactly three bonds to complement the dihedral potential. These "1-4" electrostatic interactions are computed using a direct Coulombic interaction and are hence excluded from the Ewald sum.

■ ASSOCIATED CONTENT

S Supporting Information. M.DynaMix 5.2 force field files for the studied amino acid analogs. This material is available free of charge via the Internet at http://pubs.acs.org/.

■ AUTHOR INFORMATION

Corresponding Author
*E-mail: ed@nd.edu; telephone: (574) 631-5687.

■ ACKNOWLEDGMENT

■ REFERENCES

(1) Prausnitz, J. M.; Lichtenthaler, R. N.; de Azevedo, E. G. *Molecular Thermodynamics of Fluid-phase Equilibria*, 3rd ed.; Prentice-Hall PTR: Upper Saddle River, NJ, 1999.

(2) Connors, K. A.; Mecozzi, S. *Thermodynamics of Pharmaceutical Systems: An Introduction to Theory and Applications*, 2nd ed.; John Wiley and Sons, Inc.: Hoboken, NJ, 2010.

(3) *Water-Insoluble Drug Formulation*, 2nd ed.; Liu, R., Ed.; CRC Press: Boca Raton, FL, 2008.

(4) Wade, L. G. *Organic Chemistry*, 6th ed.; Pearson Education, Inc.: Upper Saddle River, NJ, 2006.

(5) Anfinsen, C. B. *Science* **1973**, *181*, 223–230.

(6) Dill, K. A.; Ozkan, S. B.; Shell, M. S.; Weikl, T. R. *Annu. Rev. Biophys.* **2008**, *37*, 289–316.

(7) Shirts, M. R.; Pitera, J. W.; Swope, W. C.; Pande, V. S. *J. Chem. Phys.* **2003**, *119*, 5740–5761.

(8) Shirts, M. R.; Pande, V. S. *J. Chem. Phys.* **2005**, *122*, 134508.

(9) Hess, B.; van der Vegt, N. F. A. *J. Phys. Chem. B* **2006**, *110*, 17616–17626.

(10) Chang, J.; Lenhoff, A. M.; Sandler, S. I. *J. Phys. Chem. B* **2007**, *111*, 2098–2106.

(11) Mobley, D. L.; Dumont, E.; Chodera, J. D.; Dill, K. A. *J. Phys. Chem. B* **2007**, *111*, 2242–2254.

(12) Kirkwood, J. G. *J. Chem. Phys.* **1935**, *3*, 300–313.

(13) Bennett, C. H. *J. Comput. Phys.* **1976**, *22*, 245–268.

(14) Valleau, J. P.; Card, D. N. *J. Chem. Phys.* **1972**, *57*, 5457–5462.

(15) Lu, N.; Kofke, D. A. *J. Chem. Phys.* **1999**, *111*, 4414–4423.

(16) Lyubartsev, A. P.; Martsinovski, A. A.; Shevkunov, S. V.; Vorontsov-Velyaminov, P. N. *J. Chem. Phys.* **1992**, *96*, 1776–1783.

(17) Lyubartsev, A. P.; Laaksonen, A.; Vorontsov-Velyaminov, P. N. *Mol. Phys.* **1994**, *82*, 455–471.

(18) Lyubartsev, A. P.; Laaksonen, A.; Vorontsov-Velyaminov, P. N. *Mol. Sim.* **1996**, *18*, 43–58.

(19) Lyubartsev, A. P.; Forrisdahl, O. K.; Laaksonen, A. *J. Chem. Phys.* **1998**, *108*, 227–233.

(20) Aberg, K. M.; Lyubartsev, A. P.; Jacobsson, S. P.; Laaksonen, A. *J. Chem. Phys.* **2004**, *120*, 3770–3776.

(21) Shah, J. K.; Maginn, E. J. *J. Phys. Chem. B* **2005**, *109*, 10395–10405.

(22) Martinez-Veracoechea, F. J.; Escobedo, F. A. *J. Phys. Chem. B* **2008**, *112*, 8120–8128.

(23) Chang, J. *J. Chem. Phys.* **2009**, *131*, 074103.

(24) Cichowski, E. C.; Schmidt, T. R.; Errington, J. R. *Fluid Phase Equilib.* **2005**, *236*, 58–65.

(25) Paluch, A. S.; Jayaraman, S.; Shah, J. K.; Maginn, E. J. *J. Chem. Phys.* **2010**, *133*, 124504.

(26) Lyubartsev, A. P.; Jacobsson, S. P.; Sundholm, G.; Laaksonen, A. *J. Phys. Chem. B* **2001**, *105*, 7775–7782.

(27) Mobley, D. L.; Bayly, C. I.; Cooper, M. D.; Shirts, M. R.; Dill, K. A. *J. Chem. Theory Comput.* **2009**, *5*, 350–358.

(28) Wang, F.; Landau, D. P. *Phys. Rev. Lett.* **2001**, *86*, 2050–2053.

(29) Yan, Q.; Faller, R.; de Pablo, J. J. *J. Chem. Phys.* **2002**, *116*, 8745–8749.

(30) Shell, M. S.; Debenedetti, P. G.; Panagiotopoulos, A. Z. *Phys. Rev. E* **2002**, *66*, 056703.

(31) Fitzgerald, M.; Picard, R. R.; Silver, R. N. *Europhys. Lett.* **1999**, *46*, 282–287.

(32) Fitzgerald, M.; Picard, R. R.; Silver, R. N. *J. Stat. Phys.* **2000**, *98*, 321–345.

(33) Errington, J. R. *Phys. Rev. E* **2003**, *67*, 012102.

(34) Errington, J. R. *J. Chem. Phys.* **2003**, *118*, 9915–9925.

(35) Paluch, A. S.; Shen, V. K.; Errington, J. R. *Ind. Eng. Chem. Res.* **2008**, *47*, 4533–4541.

(36) Fenwick, M. K.; Escobedo, F. A. *J. Chem. Phys.* **2004**, *120*, 3066–3074.

(37) Escobedo, F. A.; Abreu, C. R. A. *J. Chem. Phys.* **2006**, *124*, 104110.

(38) Kong, X., III; C., L. B. *J. Chem. Phys.* **1996**, *105*, 2414–2423.

(39) Allen, M. P.; Tildesley, D. J. *Computer Simulation of Liquids*; Oxford University Press Inc.: New York, 1987.

(40) Torrie, G. M.; Valleau, J. P. *Chem. Phys. Lett.* **1974**, *28*, 578–581.

(41) Berg, B. A.; Neuhaus, T. *Phys. Rev. Lett.* **1992**, *68*, 9–12.

(42) Fenwick, M. K.; Escobedo, F. A. *J. Chem. Phys.* **2003**, *119*, 11998–12010.

(43) Shell, M. S.; Debenedetti, P. G.; Panagiotopoulos, A. Z. *J. Chem. Phys.* **2003**, *118*, 9406–9411.

(44) Wang, F.; Landau, D. P. *Phys. Rev. E* **2001**, *64*, 056101.

(45) Yan, Q.; de Pablo, J. J. *Phys. Rev. Lett.* **2003**, *90*, 035701.

(46) Frenkel, D.; Smit, B. *Understanding Molecular Simulation: From Algorithms to Applications*, 2nd ed.; Academic Press: San Diego, CA, 2002.

(47) Lu, N.; Singh, J. K.; Kofke, D. A. *J. Chem. Phys.* **2003**, *118*, 2977–2984.

(48) Shirts, M. R.; Bair, E.; Hooker, G.; Pande, V. S. *Phys. Rev. Lett.* **2003**, *91*, 140601.

(49) Ferrenberg, A. M.; Swendsen, R. H. *Phys. Rev. Lett.* **1989**, *63*, 1195–1198.

(50) Wu, D.; Kofke, D. A. *J. Chem. Phys.* **2005**, *123*, 054103.

(51) Wu, D.; Kofke, D. A. *J. Chem. Phys.* **2005**, *123*, 084109.

(52) Jorgensen, W. L.; Chandrasekhar, J.; Madura, J. D. *J. Chem. Phys.* **1983**, *79*, 926–935.

(53) Wang, J.; Wolf, R. M.; Caldwell, J. W.; Kollman, P. A.; Case, D. A. *J. Comput. Chem.* **2004**, *25*, 1157–1174.

(54) Wang, J.; Wang, W.; Kollman, P. A.; Case, D. A. *J. Mol. Graphics Modell.* **2006**, *25*, 247–260.

(55) Jakalian, A.; Bush, B. L.; Jack, D. B.; Bayly, C. I. *J. Comput. Chem.* **2000**, *21*, 132–146.

(56) Beutler, T. C.; Mark, A. E.; van Schaik, R. C.; Gerber, P. R.; van Gunsteren, W. F. *Chem. Phys. Lett.* **1994**, *222*, 529–539.

(57) Steinbrecher, T.; Mobley, D. L.; Case, D. A. *J. Chem. Phys.* **2007**, *127*, 214108.

(58) Lyubartsev, A. P.; Laaksonen, A. *Comput. Phys. Commun.* **2000**, *128*, 565–589.

(59) Lyubartsev, A. P.; Laaksonen, A. *MDynaMix: a Molecular Dynamics Program*; Universitet Stockholms: Stockholm, Sweden; http://www.mmk.su.se/~sasha/mdynamix/. Accessed February 1, 2010).

(60) Ryckaert, J.; Ciccotti, G.; Berendsen, H. J. C. *J. Comput. Phys.* **1977**, *23*, 327–341.

(61) Andersen, H. C. *J. Chem. Phys.* **1980**, *72*, 2384–2393.

(62) Andrea, T. A.; Swope, W. C.; Andersen, H. C. *J. Chem. Phys.* **1983**, *79*, 4576–4584.

(63) Martyna, G. J.; Tobias, D. J.; Klein, M. L. *J. Chem. Phys.* **1994**, *101*, 4177–4189.

(64) Efron, B. *SIAM Review* **1979**, *21*, 460–480.

(65) Efron, B. *Biometrika* **1981**, *68*, 589–599.

(66) Moore, D. S.; McCabe, G. P.; Craig, B. *Introduction to the Practice of Statistics*, 6th ed.; W.H. Freeman and Company: New York, 2009.

(67) Wolfenden, R.; Andersson, L.; Cullis, P. M.; Southgate, C. C. B. *Biochemistry* **1981**, *20*, 849–855.

(68) Kofke, D. A.; Cummings, P. T. *Mol. Phys.* **1997**, *92*, 973–996.

(69) Kofke, D. A.; Cummings, P. T. *Fluid Phase Equilib.* **1998**, *150–151*, 41–49.

(70) Swendsen, R. H.; Weng, J.-S. *Phys. Rev. Lett.* **1986**, *57*, 2607–2609.

(71) Hansmann, U. H. E. *Chem. Phys. Lett.* **1997**, *281*, 140–150.

(72) Earl, D. J.; Deem, M. W. *Phys. Chem. Chem. Phys.* **2005**, *7*, 3910–3916.

(73) Errington, J. R. *Langmuir* **2004**, *20*, 3798–3804.

(74) Shen, V. K.; Errington, J. R. *J. Phys. Chem. B* **2004**, *108*, 19595–19606.

(75) de Leeuw, S. W.; Perram, J. W.; Smith, E. R. *Proc. R. Soc. Lond. A* **1980**, *373*, 27–56.

(76) Heyes, D. M. *CCP5 Quarterly Newsletter* **1983**, *8*, 29–36.